Triple-Objective Optimization of an Industrial Hydrogen Plant

P. P. OH, AJAY K. RAY AND G. P. RANGAIAH
Department of Chemical and Environmental Engineering, National University of Singapore, Singapore 119260

Keywords: Hydrogen Production, Modelling and Optimization, Multiple Objectives, Optimal Heat Flux Profile, Genetic Algorithm

In this work the performance of an industrial hydrogen plant is improved by multi-objective optimization using an adaptation of the nondominated sorting genetic algorithm (NSGA). The heat flux profile on the steam reformer tubes is treated as a decision variable, yielding optimal heat flux profiles for each Pareto solution. The optimization problem has been considered both as a two and three-objective problem. For a fixed feed rate of methane to the unit, simultaneous maximization of product hydrogen and export steam flow rates are considered as the two objectives. The results are better than those obtained in an earlier work by Rajesh *et al*. (2001), with flue gas temperature in place of the heat flux profile as a decision variable. Minimization of reformer duty was chosen to be the third objective. More useful information is available for the optimal operation of hydrogen plants from three-objective optimization, even though computational time for two and three objectives is comparable.

Introduction

Hydrogen is of critical importance in the chemical and process industries where it is involved in many catalytic processes for the synthesis of intermediate products (e.g. ammonia, ethylene and methanol). Owing to some recent developments in petroleum refineries, such as a planned increase in heavy oil production, demand for clean fuels, and the reduction in the aromatic content allowed in diesels, the demand for hydrogen is expected to increase in the next ten years.

Steam reforming of natural gas is the most economical and widely used process for the production of hydrogen. Currently, about 80% of the 500 billion Nm^3 of hydrogen produced yearly in the world is obtained by this process. In addition, due to the availability of recoverable heat, hydrogen plants produce steam both for internal consumption as well as for export to other units. As the reforming reaction is strongly endothermic, energy for the reaction is supplied by combustion of natural gas or fuel oil. A large amount of heat has to be supplied to replenish the heat consumed by the reaction and to maintain the process gas at the elevated temperatures required for acceptable rates of reaction and high equilibrium conversion. The high energy input required for the process, coupled with continually increasing energy cost, makes it pertinent to operate the steam reformer in the most efficient manner under optimal conditions.

King and Bochow (2000) provided a list of the salient design and operating factors to consider when analysing a hydrogen plant. They suggested a careful evaluation of alternative hydrogen technologies before a decision is made whether to produce hydrogen in-house or to outsource hydrogen, so as to ensure long-term profitability in the competitive market. Once a hydrogen plant is built, it is essential to operate it optimally. This in turn requires rigorous modelling and optimization of hydrogen plants.

A typical hydrogen plant has two reactors—a steam reformer and a shift converter. A multitude of works on reforming and shift conversion kinetics as well as some publications on the reactor modelling and simulation aspects are available in the open literature. Among the kinetic studies on the steam reformer, a significant study is that by Xu and Froment (1989a, 1989b) who developed a rate expression based upon a 13-step adsorption-desorption mechanism model. This rate expression accounts for the contradictions found in earlier studies and correlates well with experimental and industrial data over a wide range of operating conditions. Using this kinetic model, Elnashaie and Alhabdan (1989) presented detailed reactor models for different types of industrial steam reformers. A detailed review of past works in the fields of shift conversion kinetics and reactor modelling was provided by Elnashaie and Elshishini (1993).

In comparison to many studies on reaction kinetics and reactor modelling, published papers on the optimization of hydrogen plants are very limited. These

Received on December 6, 2000. Correspondence concerning this article should be addressed to G. P. Rangaiah (E-mail address: chegpr@nus.edu.sg).

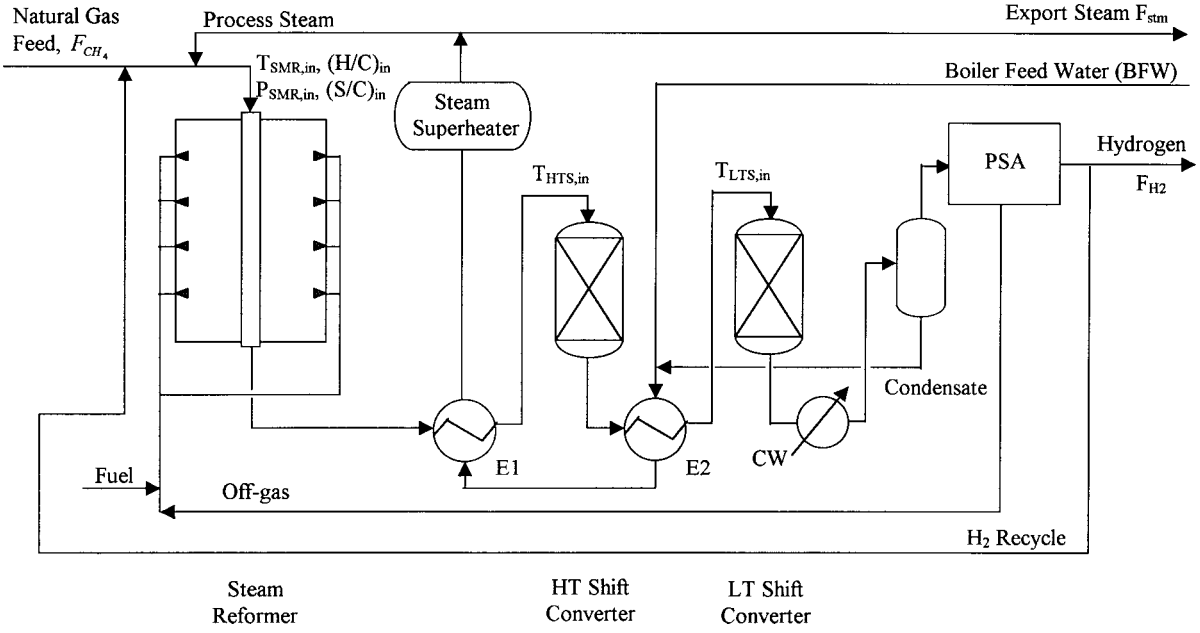

Fig. 1 Process flow diagram of a typical H_2 plant

studies are reviewed recently by Rajesh *et al.* (2000) for steam reformers and by Bhaskar *et al.* (2000a) for chemical engineering processes in general. Rajesh *et al*. (2000) also optimized the performance of a side-fired steam reformer with dual objectives of minimizing methane feed rate and maximizing the flow rate of carbon monoxide, for a fixed hydrogen production rate. Subsequently, Rajesh *et al.* (2001) added models for shift converters and steam generators to develop the complete model for an industrial hydrogen plant. The complete model was then used to obtain optimal operating conditions for a complete hydrogen plant by considering simultaneous maximization of product hydrogen and export steam flow rates for a fixed methane feed rate.

In addition to maximizing hydrogen and steam production, minimizing the total heat duty of the steam reformer is also important for the optimal operation of industrial hydrogen plants. Rajesh *et al*. (2000, 2001) considered furnace gas temperature in the reformer as one of the decision variables. In a side-fired furnace, it is possible to select firing of the burners so as to achieve a specified heat flux on reformer tubes (Rostrup-Nielsen, 1984). Hence, heat flux profile can be considered as one of the decision variables (instead of furnace gas temperature). This will provide scope for improving the hydrogen plant operation even further. In this work, optimal operation of an industrial hydrogen plant is studied by including both these aspects (namely, the third objective and the heat flux profile in the steam reformer). A genetic algorithm (GA) is employed for solving the multi-objective optimization problem. Findings of this study are described and compared with the earlier results.

1. Process Description

The process flow sheet of a typical hydrogen plant is shown in **Fig. 1**. Natural gas (assumed to contain methane only and no other hydrocarbons) is mixed with appropriate quantities of steam and recycle H_2 before it is fed into the reformer furnace. Recycle of a part of the product H_2 to the feed is required to maintain the catalyst in the earlier sections of the reformer tubes in its active state. A surplus of steam over its stoichiometric ratio reduces CH_4 leakage from the reformer and improves CO conversion in the shift converters. A high steam to carbon ratio also helps to avoid coke formation. The main reactions occurring in the reformer are:

$$CH_4 + H_2O \rightleftarrows CO + 3H_2$$
$$-\Delta H_r = -2.061 \times 10^5 \quad \text{[kcal/kmol]} \quad (1)$$

$$CO + H_2O \rightleftarrows CO_2 + H_2$$
$$-\Delta H_r = +4.11 \times 10^4 \quad \text{[kcal/kmol]} \quad (2)$$

$$CH_4 + 2H_2O \rightleftarrows CO_2 + 4H_2$$
$$-\Delta H_r = -1.650 \times 10^5 \quad \text{[kcal/kmol]} \quad (3)$$

The hot syngas exiting the reformer undergoes heat exchange with preheated boiler feed water (BFW) to produce very high-pressure (VHP) steam, part of which is used for mixing with the feed (internal use),

and the remainder for export outside the unit. The exothermic shift reaction (Eq. (2)) takes place predominantly in the high temperature (HT) and low temperature (LT) shift converters to produce additional H_2. The surplus heat in the process gas leaving the HT shift converter is used to preheat BFW before it undergoes further reaction in the LT shift converter. The H_2-rich stream exiting the LT shift converter is cooled and flashed to remove excess steam as condensate, which is recycled back into the process. Thereafter, H_2 is separated from the off-gases in a pressure-swing adsorption (PSA) unit. The off-gas, along with additional fuel, is used for combustion in the reformer furnace.

2. Reformer Model and Simulation

The model of the hydrogen plant used in this work is similar to that reported by Rajesh *et al*. (2001). They incorporated the rate expression developed by Xu and Froment (1989a), the heat transfer model of Singh and Saraf (1979) for side-fired steam reformers, and the simplified model II of Elnashaie and Elshishini (1993) for intra-pellet calculations, in the reformer model. The intra-pellet concentration profiles and the effectiveness factor at an axial location in the reaction were solved using the method of orthogonal collocation on finite elements (OCFE). The shift converter model used is similar to that of Elnashaie and Alhabdan (1989). The quantity of steam produced from process gas heat was obtained from an energy balance on E1 and E2 (Fig. 1). The steam separator was modelled as an isothermal flash of the process gas that is cooled to room temperature. The PSA unit was simulated as a "black box" with 90% hydrogen recovery and 99.95% hydrogen purity in the product. This can be justified in view of the fact that, for nominal perturbations in PSA feed composition and pressure, desired H_2 yield and purity can be attained by making minor adjustments to adsorption/desorption cycle times in the PSA unit (Chlendi *et al*., 1995). The reader is referred to the works of Rajesh *et al*. (2000, 2001) for a detailed description of all the model equations.

While adapting the model described above for our work, a programming error, which resulted in steam generation being disproportionate to the heat load on the waste-heat exchangers E1 and E2 (Fig. 1), was uncovered. Upon correction, steam generation from process heat recovery was found to be barely sufficient to supply internal process use, with little excess available for export outside the unit. A shortcoming of the model of Rajesh *et al.* (2001) lies in the fact that it fails to account for steam generation based on heat recovery from exiting flue gases. In typical industrial units, this source accounts for about 60% of total steam generation. In this work, total steam generation is found based on the assumption that steam produced from process heat (found from energy balance on E1 and E2) accounts for 40% of the total. Subsequently, the quantity of steam available for export was determined by subtracting that needed for mixing with methane feed from the total.

In addition, two modifications were made to the model of the steam reformer. Rajesh *et al*. (2000, 2001) assumed the furnace gas temperature to be constant throughout the length of the reformer tubes. The model equations of Singh and Saraf (1979) were then solved together with a heat balance equation to compute the tube wall and process gas temperatures, and heat flux on the reformer tube surface at any axial location. In this work the reformer axial heat flux profile is expressed as a function of reformer tube length. The set of equations for heat transfer from the furnace to the tubes was then adapted to solve for the tube wall and process gas temperatures in conjunction with the heat balance.

The second modification is with regard to improving computational efficiency. When performing intra-pellet calculations to evaluate effectiveness factors for the reactions occurring in the reformer, the catalyst pellet was modelled as a slab with two finite elements extending over $0 \le \nu \le 0.2$ (outer region) and $0.2 \le \nu \le 1.0$ (inner region). The component fluxes are assumed to be zero at $\nu = 0.2$, implying that the entire inner region of the catalyst slab exists in equilibrium. In this work, ten, instead of the original eighteen, orthogonal collocation (OC) points were used in the first finite element (outer region). The model was simulated on the CRAY J916 supercomputer using the mathematical routines IVPAG (for integration of stiff ordinary differential equations) and NEQNF (for solving the nonlinear set of algebraic collocation equations) available in IMSL (International Mathematics & Statistics Libraries). With ten OC points, one complete simulation of the hydrogen plant required 1.58 seconds of CPU time on a CRAY J916 supercomputer, as compared to 1.66 seconds with eighteen points. The simulation results differed by less than 1%, justifying the use of a smaller number of OC points to improve computational efficiency, which would save overall CPU time for optimization.

3. Formulation of the Optimization Problem

3.1 Optimization problem for two objective functions

For a fixed feed rate of methane, F_{CH_4}, to the hydrogen plant, the value of the product hydrogen, the price that the export steam can fetch, and the cost of furnace fuel required to fire the reformer will determine the profitability of the plant. In the absence of generalised cost data, the search for optimal operating conditions for the hydrogen plant is thus inherently a

multi-objective optimization problem. Simultaneous maximization of the flow rates of product hydrogen, F_{H_2}, and export steam, F_{stm}, is first considered.

The optimization problem can be formulated as:

Maximize:

$$J_1 = F_{H_2} \tag{4}$$

$$J_2 = F_{stm} \tag{5}$$

Subject to:

$$T_{w,max} \le 1200 \quad [K] \tag{6}$$

$$\left[\frac{y_{H_2O}}{y_{H_2}}\right]_{HTS} \ge 0.3 \tag{7}$$

$$T_{LTS} \ge (T_{dew} + 15) \quad [K] \tag{8}$$

$$Q_{Ei} \le 1.2 \times Q_{Ei\,max} \quad (i = 1, 2) \tag{9}$$

$$F \le 1.2 \times F_{max} \tag{10}$$

$$\frac{Q_{fuel}}{Q_{SMR}} \le \alpha \tag{11}$$

where α is a constant to be discussed below.

Equation (6) is based on the creep limit of alloy steel tubes at operating conditions. The (H_2O/H_2) molar ratio in the high temperature shift (HTS) converter (Eq. (7)) should be maintained above 0.3 to prevent methanation reactions from occurring within the reactor. The process gas temperature in the low temperature shift (LTS) converter (Eq. (8)) should be at least 15°C above the dew point of the bulk gas to ensure that steam does not condense within the catalyst pores, which can result in catalyst deactivation. The heat duties of the heat exchangers (Eq. (9)) and the total unit feed rate to the reformer (Eq. (10)) must be constrained within allowable design margins. Finally, an upper bound is given on the fraction of the reformer duty, Q_{SMR}, supplied by external fuel, Q_{fuel} (Eq. (11)). With this constraint, a variety of operating scenarios can be obtained by performing the optimization with different values of α. Two values of α are considered, namely, 0.60 (reference case) and 0.55, consistent with values typically encountered in industrial practice.

The axial heat flux profile (referred to the outer surface), q, in the reformer is expressed as a function of tube length, z. The heat flux profile in a typical industrial furnace is parabolic and peaks in the early part of the reformer tubes (Rostrup-Nielsen, 1984). It is thus modelled with two quadratic functions defined for the sections of the reformer tubes preceding and following the point, z^* where the heat flux is at the maximum.

For $z \le z^*$

$$q = A + B\left(\frac{z}{z^*}\right) + C\left(\frac{z}{z^*}\right)^2 \tag{12a}$$

For $z > z^*$

$$q = A + B + C + D\left(\frac{z - z^*}{L}\right) + E\left(\frac{z - z^*}{L}\right)^2 \tag{12b}$$

where L is the total tube length. Thus specifying the heat flux profiles involves the coefficients A to E and z^* in the above equations.

Thus the optimization problem for the hydrogen plant has twelve decision variables. Ten of them (Eqs. (13a)–(13j)) account for the inlet gas temperature, pressure and gas composition at the reformer inlet, as well as the heat flux profile on the reformer tubes. The remaining two variables (Eqs. (13k) and (13l)) specify the inlet temperatures to the adiabatic shift converters. The following bounds are used for the decision variables:

$$725 \le T_{SMR,in} \le 900 \quad [K] \tag{13a}$$

$$2450 \le P_{SMR,in} \le 2950 \quad [kPa] \tag{13b}$$

$$2.0 \le (S/C)_{in} \le 6.0 \tag{13c}$$

$$0.0 \le (H/C)_{in} \le 0.5 \tag{13d}$$

$$20 \le A \le 80 \quad [Mcal\ m^{-2}h^{-1}] \tag{13e}$$

$$0 \le B \le 60 \quad [Mcal\ m^{-2}h^{-1}] \tag{13f}$$

$$-30 \le C \le 0 \quad [Mcal\ m^{-2}h^{-1}] \tag{13g}$$

$$-60 \le D \le 0 \quad [Mcal\ m^{-2}h^{-1}] \tag{13h}$$

$$-60 \le E \le 30 \quad [Mcal\ m^{-2}h^{-1}] \tag{13i}$$

$$0.5 \le z^* \le 2.0 \tag{13j}$$

$$570 \le T_{HTS,in} \le 730 \quad [K] \tag{13k}$$

$$400 \le T_{LTS,in} \le 530 \quad [K] \tag{13l}$$

The lower and upper bounds on $T_{SMR,in}$ are based, respectively, on thermodynamic limitations to prevent gum formation on the reformer catalyst and on the maximum heat that the feed can usually pick up from the flue gas in the convection section of the reforming furnace. The minimum and maximum values of $P_{SMR,in}$

are decided by the normal pressure at which H_2 is to be produced in the plant and the supply pressure of the natural gas feed. Bounds on $T_{HTS,in}$ and $T_{LTS,in}$ are decided based on normal operating ranges in industrial units. A very low value of $(S/C)_{in}$ will result in carbon formation on the reformer catalyst leading to tube damage or rupture, whilst an excessively high value is uneconomical owing to the unnecessary heating of the excess steam which is subsequently condensed downstream of the reformer. For these reasons, the value of $(S/C)_{in}$ is restricted to between 2.0 and 6.0. The upper limit on $(H/C)_{in}$ is selected to avoid redundant H_2 recycle to the reformer.

The reformer tube is highly susceptible to creep damage caused by thermal stresses resulting from the temperature difference over the tube wall, thus limiting the maximum allowable heat flux for a given wall temperature (Rostrup-Nielsen, 1984). Bounds on q have been fixed between 20 and 80 Mcal $m^{-2}h^{-1}$ based on industrial experience. The bounds on A correspond to these on q. The limits on variables B to E ensure maximum scope in the selection of a optimum heat flux profile while satisfying the specified bounds for q and conforming to the constraint of zero gradient at the turning point, z^*. The range of values for z^* are based on typical heat flux profiles in industrial reformers (Rostrup-Nielsen, 1984).

Since the optimization program is for minimization, maximization of F_{H_2} and F_{stm} is expressed as minimization of the corresponding reciprocal quantities. Also, the performance constraints (Eqs. (6)–(11)) were incorporated into the objective functions as penalty functions. Thus the optimization problem studied becomes

$$I_1 = \frac{10^3}{F_{H_2}} + 10^4 \cdot \sum_{i=1}^{7} f_i \tag{14}$$

$$I_2 = \frac{10^3}{F_{stm}} + 10^4 \cdot \sum_{i=1}^{7} f_i \tag{15}$$

where

$$f_1 = (T_{w,max} - 1200) + |T_{w,max} - 1200| \tag{16a}$$

$$f_2 = \left[0.3 - \frac{y_{H_2O}}{y_{H_2}}\right] + \left|0.3 - \frac{y_{H_2O}}{y_{H_2}}\right| \tag{16b}$$

$$f_3 = [(T_{dew} + 15) - T_{LTS}] + |(T_{dew} + 15) - T_{LTS}| \tag{16c}$$

$$f_4 = (Q_{E1} - 1.2Q_{E1\,max}) + |Q_{E1} - 1.2Q_{E1\,max}| \tag{16d}$$

$$f_5 = (Q_{E2} - 1.2Q_{E2\,max}) + |Q_{E2} - 1.2Q_{E2\,max}| \tag{16e}$$

$$f_6 = (F - 1.2F_{max}) + |F - 1.2F_{max}| \tag{16f}$$

$$f_7 = \left[\frac{Q_{fuel}}{Q_{SMR}} - \alpha\right] + \left|\frac{Q_{fuel}}{Q_{SMR}} - \alpha\right| \tag{16g}$$

The numerical weighting factors used in Eqs. (14) and (15) give a similar range in magnitude of values for the objective functions to avoid numerical problems.

3.2 Optimization problem for three objective functions

The optimization problem outlined above is also solved by considering three objective functions. Maximizing the flow rates of product hydrogen, F_{H_2}, and export steam, F_{stm}, remain as the first two objectives. Some consideration has to be given to the selection of the third objective. The heat duty required by the reformer, Q_{SMR}, is supplied partially by the off-gas from the PSA unit, with the deficit provided for by additional fuel. The cost of furnace fuel is one of the factors that govern the economics of the plant. The heating value of the PSA off-gas increases with the extent of methane leakage from the reformer. It therefore follows that high methane leakage from the reformer would increase the heating value of the PSA off-gas and has the effect of lowering the requirement for external fuel at the expense of H_2 production and steam generation. Thus, minimization of the consumption of external fuel, Q_{fuel}, should not be chosen as an objective if the artificial lowering of fuel consumption, by favouring high methane leakage from the reformer, is to be avoided. Hence, minimizing the total heat duty of the reformer, Q_{SMR}, is taken as the third objective so as to obtain the most energy efficient operating scenarios. Note that Q_{SMR} is calculated by integrating the heat flux on the reformer tubes along the tube length. The third objective can be written as:

Minimize:

$$J_3 = Q_{SMR} \tag{17}$$

or, incorporating the penalty functions

$$I_3 = \frac{Q_{SMR}}{10^2} + 10^4 \cdot \sum_{i=1}^{7} f_i \tag{18}$$

A slight modification is made to the constraint on the reformer duty, Q_{SMR}, supplied by external fuel, Q_{fuel} (Eq. (11)). Here, the constraint is given as

$$\frac{Q_{fuel}}{Q_{SMR}} \geq 0.55 \tag{19}$$

The contribution by external fuel is restricted to above 55%. In the absence of this constraint, the practically impossible scenario of negative Q_{fuel}/Q_{SMR} was encountered during optimization. This is derived from the manner in which Q_{fuel} is calculated in the program. Q_{fuel} is found from a difference between the total reformer heat duty and the heat duty available in the PSA off-gas. An excessively high methane leakage from the reformer will result in the heat duty in the PSA off-gas being more than sufficient to provide for the reformer, hence resulting in negative Q_{fuel}. In such operating scenarios, Q_{SMR} tends to be very low as only minimal heat needs to be supplied to the reforming furnace. These scenarios are thus considered "optimal" when Q_{SMR} is to be minimized. Therefore, the above constraint is essential to exclude optimal solutions which give an impracticably low fuel consumption at the expense of H_2 production and steam generation. The value of the constraint is consistent with typical industrial values.

The optimization problems with both two and three objective functions are solved using an adaptation of genetic algorithm, the nondominated sorting genetic algorithm (NSGA), suitable for multi-objective problems. Apart from the works of Rajesh *et al*. (2000, 2001) and Bhaskar *et al*. (2000b) mentioned earlier, Garg and Gupta (1999) and Mitra *et al*. (1998) also have successfully employed this technique. Besides the NSGA, other forms of GAs have also been successfully used for multi-objective optimization. Hence we believe that GA is appropriate and capable of solving multi-objective optimization problems. Brief description of the NSGA is given in the Appendix while full details on the NSGA are available in Srinivas and Deb (1995) and Bhaskar *et al.* (2000a). The NSGA parameters used in this work, with the exception of the number of generations, can be found in Rajesh *et al*. (2000).

4. Results and Discussion

When an optimization problem involves two or more objective functions that are influenced in conflicting directions by changes in some of the decision variables, a set of nondominating solutions (Pareto-optimal solutions) will be obtained. A Pareto set has the property that when we move from any one point on the set to another, one or more objective functions improve while the others worsen. Hence neither solution dominates over the other and both are equally good. The process engineer will select a final solution from the Pareto set based on subjective criteria.

While performing the optimization, the limits for $(S/C)_{in}$ had to be modified based on a given $T_{SMR,in}$ inlet temperature and $(H/C)_{in}$ to avoid numerical problems during iterative computations. The mapping of $(S/C)_{in}$ from the binary chromosomes to the decimal system in the NSGA is performed using these limits rather than

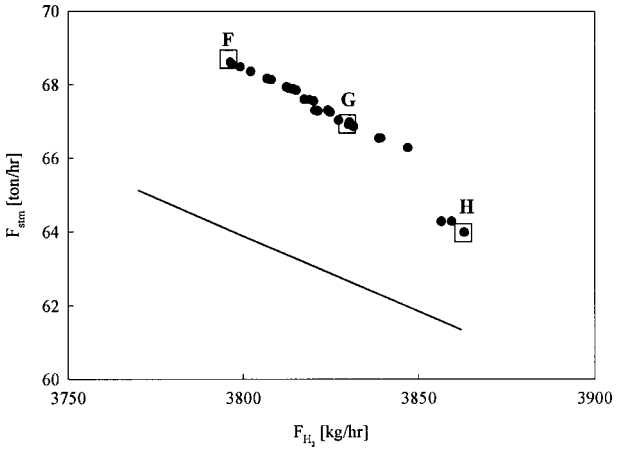

Fig. 2 Pareto-optimal set obtained for two objectives. Points represent solutions obtained with the reformer heat flux profile as a decision variable, while the solid line represents that obtained with T_g (Rajesh *et al*., 2001) as a decision variable

the ones in Eq. (13c). These modified limits still satisfy the bounds on $(S/C)_{in}$ given in Eq. (13c) as they correspond to a narrower range. However, these combinations of $T_{SMR,in}$, $(S/C)_{in}$ and $(H/C)_{in}$ avoid computational difficulties. The reader is referred to Rajesh *et al*. (2000) for more details on this.

Owing to the wide range allowed for the variables B to E (Eqs. (13f)–(13i)), randomly selected combinations of these variables have a high tendency to result in heat flux profiles which violate the restrictions on Q. To avoid this problem, the limits on B through E were modified based on the values of other decision variables. The redefined bounds are as follows:

$$0 \le B \le (80 - A) \quad [\text{Mcal m}^{-2}\text{h}^{-1}] \quad (20a)$$

$$-0.5B \le C \le 0 \quad [\text{Mcal m}^{-2}\text{h}^{-1}] \quad (20b)$$

$$(20 - A - B - C) \le D \le 0 \quad [\text{Mcal m}^{-2}\text{h}^{-1}] \quad (20c)$$

$$(20 - A - B - C - D) \le E \le -0.5D \quad [\text{Mcal m}^{-2}\text{h}^{-1}] \quad (20d)$$

These bounds have been selected to ensure that the values of B through E fall within the limits given in Eqs. (13e)–(13i) and that the heat flux profile saturates appropriately at the peak. Similar to the case of $(S/C)_{in}$, the mapping of the binary chromosomes to the decimal system in the NSGA is performed using the bounds in Eqs. (20a)–(20d) rather than those in Eqs. (13f)–(13i).

4.1 Optimization for two objective functions

Figure 2 shows the Pareto set of optimal solutions obtained after 150 generations using the two objective functions defined in Eqs. (14) and (15), with a

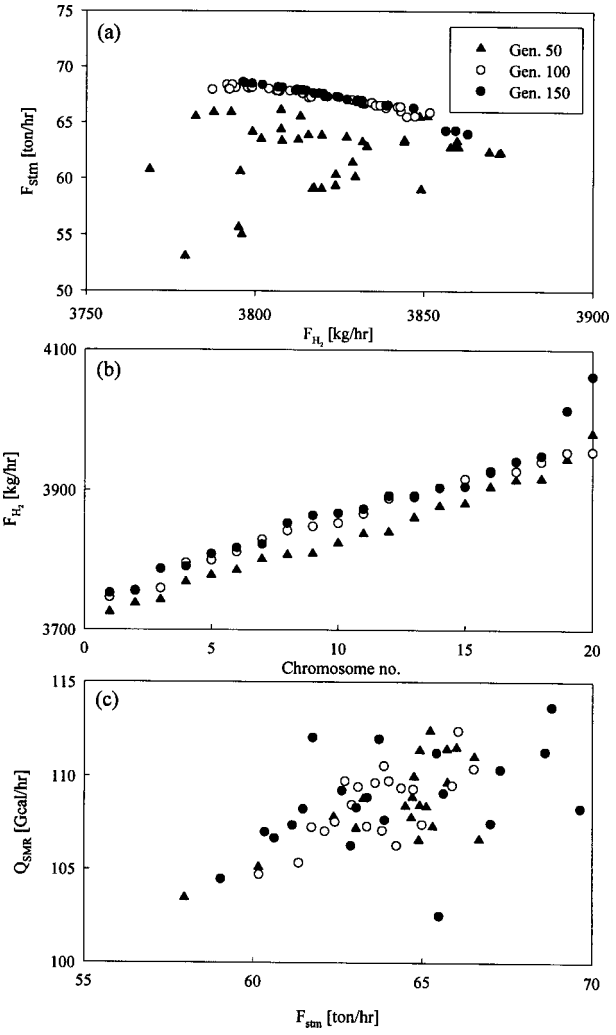

Fig. 3 Evolution of the Pareto with generation number. (a) is for two objectives, while (b) and (c) are for three objectives

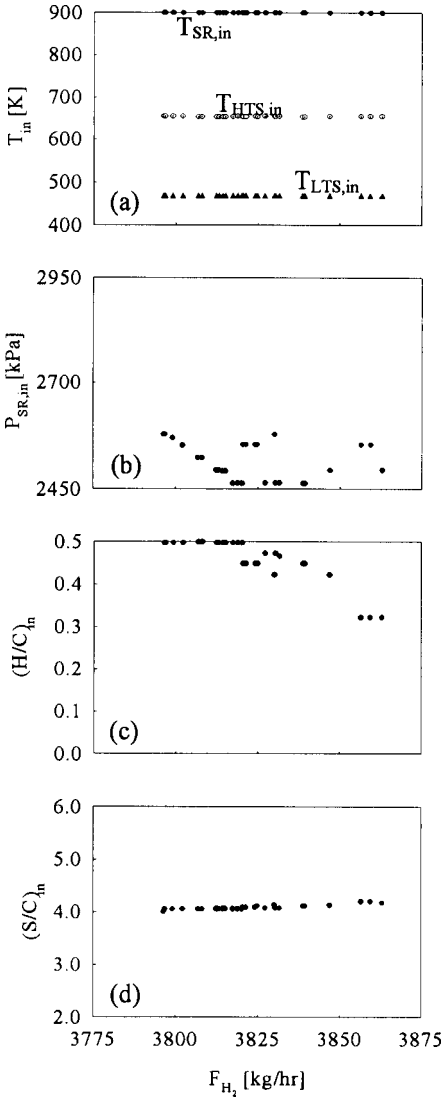

Fig. 4 Decision variables for the Pareto-optimal set in Fig. 2 for two objectives with the reformer heat flux profile as a decision variable

constraint on the reformer duty supplied by external fuel (α = 0.60 in Eq. (11)). The CPU time taken to generate one Pareto set is 12 min on the CRAY machine. **Figure 3(a)** shows the evolution of the Pareto set with the generation number. With an increase in the generation number, both objectives are improved and the Pareto set is less scattered. The negligible difference in the Pareto sets obtained at 100 and 150 generations suggests that little improvement can be achieved by performing the optimization beyond 150 generations, and indicates that convergence has been attained at 150 generations. The decision variables associated with all the points (referred to as chromosomes) on the Pareto set are shown in **Fig. 4**. **Table 1** lists the operating parameters corresponding to three selected chromosomes, *F*, *G* and *H*, on the Pareto set.

$(H/C)_{in}$ and $(S/C)_{in}$ are observed to have conflicting effects on the two objectives (Figs. 4(c) and (d)). A high $(H/C)_{in}$ inhibits the reforming reactions, lowering methane conversion and H_2 production. However, it also generates more CO in the process gas at the reformer outlet, allowing for a more exothermic reaction in the shift converters, resulting in increased steam generation. A large value of $(S/C)_{in}$ increases methane conversion, leading to greater H_2 production, but also reduces CO production in the reformer and hence steam generation. Therefore, a combination of low $(H/C)_{in}$ and high $(S/C)_{in}$ will result in greater H_2 production, while a high $(H/C)_{in}$ coupled with a low $(S/C)_{in}$ will yield more export steam. The small degree of scatter observed in the values of $(H/C)_{in}$ and $(S/C)_{in}$ for different values of F_{H_2} may be attributed to the slight difference in the optimal heat flux profiles.

The reforming reactions (Eqs. (1) and (3)) are favoured at high temperatures and low pressures. Under these conditions, more H_2 production and greater steam

Table 1 Operating parameters for selected chromosomes of the Pareto set in Fig. 2 for two objectives

Parameter	Chromosome F	Chromosome G	Chromosome H
$T_{SMR,in}$ [K]	899.9	899.9	899.9
$P_{SMR,in}$ [kPa]	2577.9	2577.4	2493.9
$(H/C)_{in}$	0.497	0.422	0.322
$(S/C)_{in}$	4.00	4.13	4.18
$T_{HTS,in}$ [K]	654.5	654.5	654.5
$T_{LTS,in}$ [K]	467.1	467.1	467.1
A [Mcal/m^2/hr]	74.356	74.349	73.294
B [Mcal/m^2/hr]	2.807	2.811	3.334
C [Mcal/m^2/hr]	–0.0075	–0.0019	–0.0023
D [Mcal/m^2/hr]	–35.746	–35.747	–35.414
E [Mcal/m^2/hr]	7.925	8.000	7.926
z^* [m]	1.25	1.25	1.25
F_{H_2} [kg/hr]	3796	3830	3862.9
F_{stm} [ton/hr]	68.6	66.9	64.0
Q_{SMR} [Gcal/hr]	108.9	108.8	108.0
Q_{fuel} [Gcal/hr]	64.0	64.7	64.7
Q_{fuel}/Q_{ref} [%]	58.8	59.5	59.9

generation may be obtained. As such, the optimized solutions suggest operation near the upper and lower bounds of $T_{SMR,in}$ (Fig. 4(a)) and $P_{SMR,in}$ (Fig. 4(b)), respectively. On the other hand, the shift reaction (Eq. (2)) is favoured at low temperatures and unaffected by pressure. However, the optimized values of $T_{HTS,in}$ and $T_{LTS,in}$ (Fig. 4(a)) do not fall near their lower bounds as expected. This is attributed to the constraints on the heat duties of the two exchangers downstream of the reformer, Eq. (9), which limit $T_{HTS,in}$ and $T_{LTS,in}$ according to the temperature of the process gas at the reformer outlet. Since the above variables influence the objective functions in the same manner, their values remain relatively unchanged from one chromosome to another, implying that these parameters may well be excluded as decision variables when performing optimization. However, the optimal values of $T_{SMR,in}$, $P_{SMR,in}$, $T_{HTS,in}$, $T_{LTS,in}$ depend on a specified methane feed rate, allowable wall heat flux, maximum allowable tube wall temperature, and a prescribed value of catalyst activity, all of which are variant with time. Therefore, these four variables should be retained as decision variables so as to obtain the proper optimal solutions. Some scatter can be seen in the optimal values of $P_{SMR,in}$, indicating its effect on the objective functions to be insensitive. This observation was found to be true when simulations were performed using different $P_{SMR,in}$ while keeping all other operating variables constant.

The optimized values of the variables defining the heat flux profile remain relatively invariant among the chromosomes (see values of A to E and z^* for the selected chromosomes in Table 1). There is a small degree of variation in C, which controls the curvature of the profile prior to z^*, but its effect on the overall profile is insignificant. Therefore, the same optimal heat flux pattern (**Fig. 5**) applies to the entire Pareto-optimal set. It is logical to fire the reforming furnace according to the heat demanded by the endothermic reactions taking place within the tubes. Accordingly, a high heat flux should be supplied in the initial part of the reformer tube where most of the reactions take

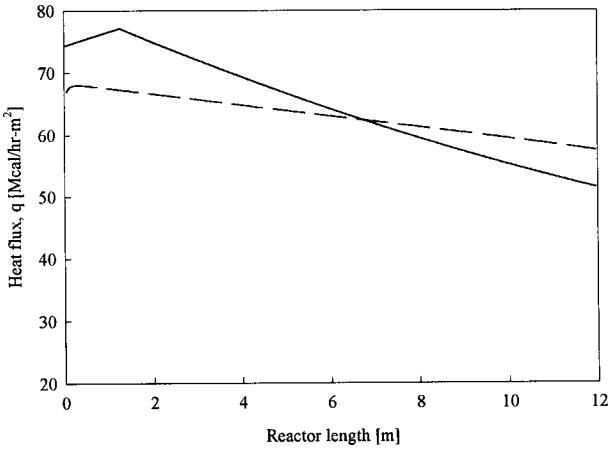

Fig. 5 Heat flux profiles on the reformer tubes for the chromosomes of the Pareto-optimal set in Fig. 2 (solid line), and for the case of T_g as a decision variable (dashed line)

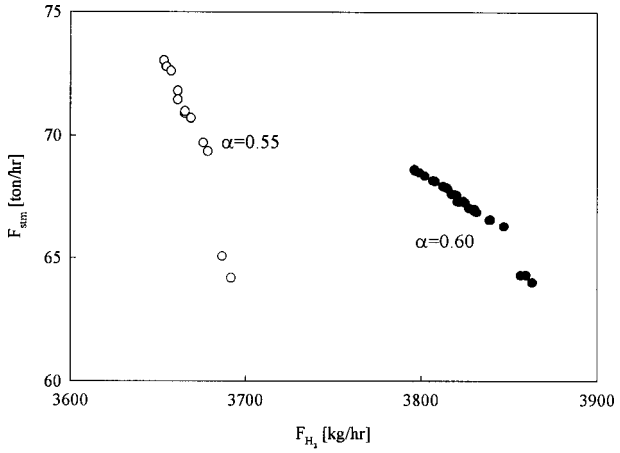

Fig. 6 Pareto-optimal sets obtained with different limits on the fraction of reformer heat duty, Q_{SMR}, supplied by external fuel

place, while a lower heat flux will suffice in the later part of the tube length. The optimized heat flux profile confirms this analysis by providing the maximum possible heat flux in the first two meters of the reformer tube, followed by a rapidly diminishing heat flux in the later section of the tube. It should be possible to achieve this profile by adjusting the firing of the burners in the reformer furnace.

The set of optimal solutions (corrected for the error in the steam generation model and assuming heat recovery from flue gas contributes to 60% of total steam generation) obtained by Rajesh *et al*. (2001) for the same objective functions with the reformer furnace gas temperature, T_g (instead of A to E and z^* defining the heat flux profile) as a decision variable is represented on Fig. 2. It is apparent from this figure that significant improvement in the objectives can be obtained by replacing T_g with the heat flux profile. The reformer heat flux profile corresponding to a typical chromosome in the Pareto set with T_g variable (Fig. 2) is presented in Fig. 5. This heat flux profile is representative of all the chromosomes in the Pareto set as it is relatively invariant from one chromosome to another. The optimal heat flux profile requires about 15% more heat flux in the initial part of the tube compared to the result of Rajesh *et al*. (2001). However, the operating scenario associated with the former requires an average reformer duty of approximately 3% more when compared with the previous case. As discussed earlier, cost of additional fuel required to supply the reformer duty has a direct bearing on the economics of the H_2 plant. It is thus logical to search for operating scenarios that are more economical on reformer duty, and hence fuel consumption. This can be achieved by performing optimization with a different upper bound on the reformer duty supplied by external fuel (Eq. (11)). By reducing the contribution of external fuel to the reformer duty, more of the requisite duty will have to be supplied by combustion of PSA off-gas. As the heat duty available in this stream is limited, the constraint will have the effect of lowering the reformer duty.

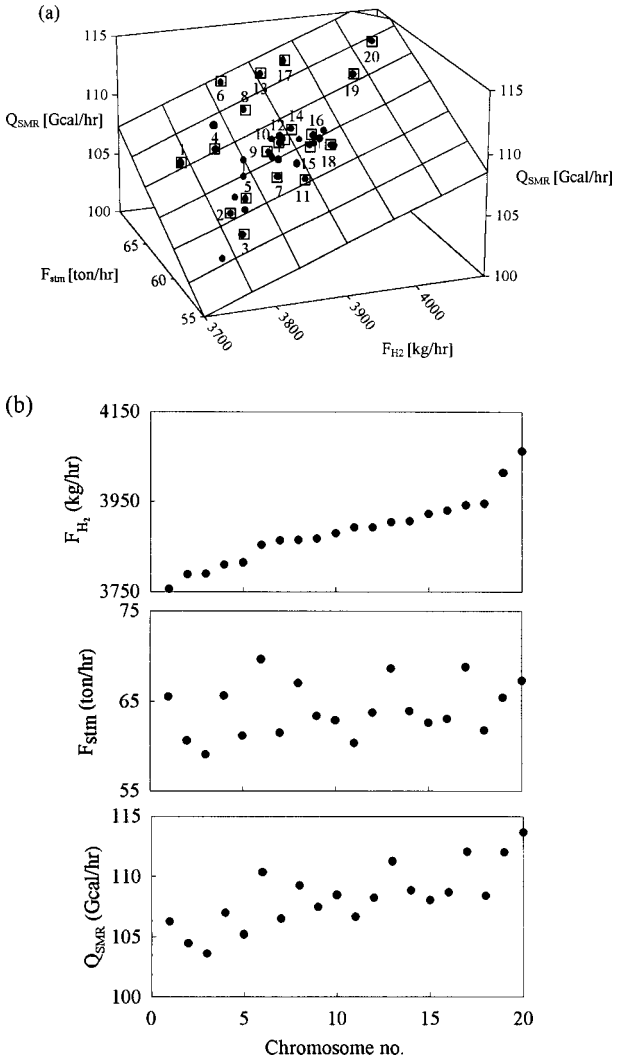

Fig. 7 Pareto-optimal set obtained for three-objectives. Points in (a) represent chromosomes, while the wire frame represents a best-fit plane, whereas in (b) 20 selected chromosomes are plotted in three 2-D plots

Figure 6 shows the Pareto optimal sets obtained by varying the constraint on the reformer duty supplied by external fuel. As the upper bound on the constraint, α, is lowered, H_2 production as well as reformer duty are reduced. (The average Q_{SMR} for the Pareto set is 108.8 Gcal/hr for α = 0.60, and 106.3 Gcal/hr for α = 0.55.) A series of optimization runs may be performed, with different values of α, to obtain all the possible operating scenarios. It would, however, be more convenient and economical on computational time to perform a single multi-objective optimization study with the inclusion of the minimization of reformer duty as the third objective, as described below.

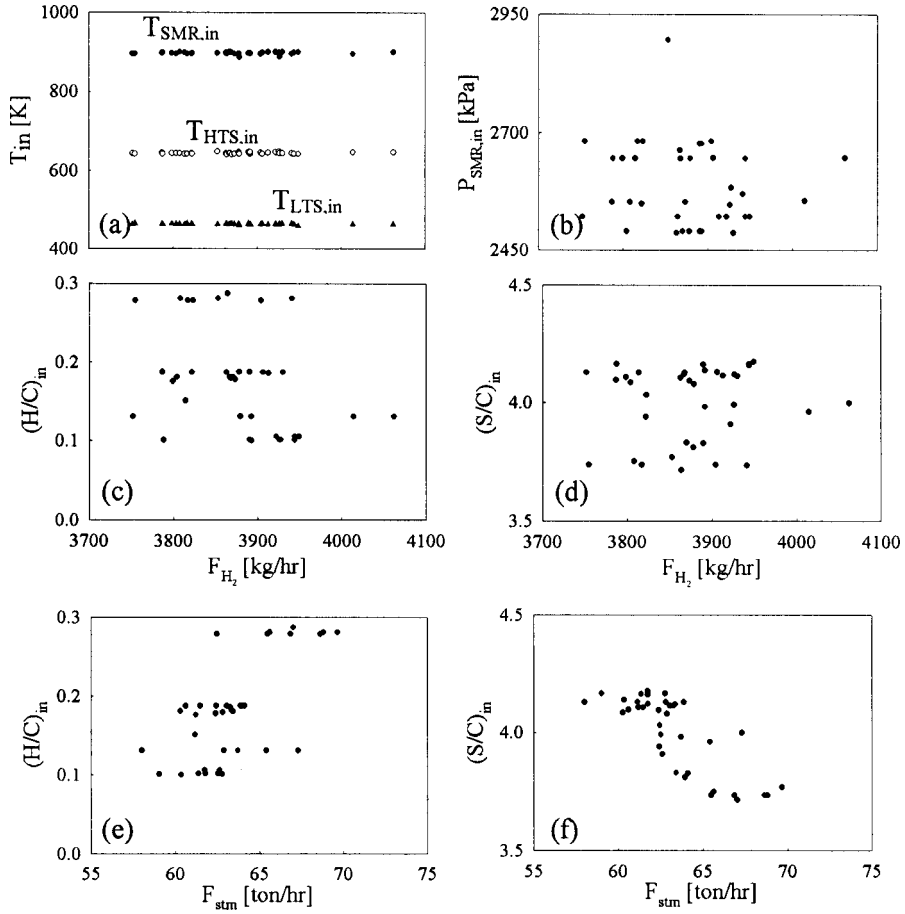

Fig. 8 Decision variables for the Pareto-optimal solutions shown in Fig. 7 for three objectives. $(H/C)_{in}$ and $(S/C)_{in}$ are plotted against F_{H_2} in (c) and (d), and against F_{stm} in (e) and (f)

4.2 Optimization for three objective functions

Optimization is performed by considering three objectives (Eqs. (4), (5) and (17)) simultaneously, with the reformer duty supplied by external fuel restricted to above 55% (Eq. (19)). **Figure 7**(**a**) shows, in three dimensions, the Pareto front obtained after 150 generations. For better clarity, plots of chromosome number in the abscissa against the value of each objective function in the ordinate axis for 20 selected chromosomes from the solution set, are also shown in Fig. 7(**b**). It can be easily observed from these plots that, as we move from one optimal point to another, one or more objectives will improve while the others worsen. For instance, chromosome 2 is superior to chromosome 1 in terms of higher H_2 production and lower reformer duty, but inferior in regard to reduced steam generation. Hence neither chromosome dominates over the other, and they are both equally good. The CPU time taken to generate one Pareto set is 12 min on the CRAY machine, identical to that required with two objective functions for 150 generations. It is thus advantageous to perform optimization with three objective functions since more useful information can be obtained with no additional computational time. Figures 3(**b**) and (**c**) show the effect of the generation number on the objectives. Operating scenarios producing more hydrogen and steam can be found with an increased number of generations. However, as no improvement can be achieved in the objectives between 100 and 150 generations, the optimization is assumed to have converged at 150 generations, and all further optimization runs are performed for this generation number.

The decision variables associated with the chromosomes in the Pareto set of Fig. 7, are illustrated in **Fig. 8**. **Table 2** lists the operating parameters corresponding to two chromosomes, 3 and 16, on the Pareto set. The optimized solutions suggest operation near the upper and lower bounds of $T_{SMR,in}$ (Fig. 8(a)) and $P_{SMR,in}$ (Fig. 8(b)), while the values of $T_{HTS,in}$ and $T_{LTS,in}$ are the lowest attainable while still satisfying the constraints on the exchanger heat duties (Eq. (9)). This is consistent with the results obtained with two objective functions. The scatter in the optimal values of $P_{SMR,in}$ suggests its effect on the objective functions to be insensitive.

Table 2 Operating parameters for selected chromosomes of the Pareto sets in Figs. 7, 10, 11 and 12 for three objectives

Parameter	Chromosome						
	3 (base case)	16 (base case)	J (F_{CH_4} = 0.9*base)	K (F_{CH_4} = 1.1*base)	L ($T_{w,max}$ < 1100 K)	M ($T_{w,max}$ < 1150 K)	N (deactivated catalyst)
$T_{SMR,in}$ [K]	898.8	898.8	891.1	899.0	899.1	897.5	899.5
$P_{SMR,in}$ [kPa]	2645.4	2645.4	2464.3	2493.0	2545.1	2488.8	2521.6
$(H/C)_{in}$	0.101	0.101	0.102	0.188	0.169	0.131	0.186
$(S/C)_{in}$	4.16	4.16	3.81	3.81	5.65	4.54	4.11
$T_{HTS,in}$ [K]	642.4	642.4	652.6	674.6	690.3	658.1	644.9
$T_{LTS,in}$ [K]	462.6	462.6	472.2	500.9	523.2	499.0	462.6
A [Mcal/m^2/hr]	73.444	73.226	69.708	78.732	79.576	72.059	73.347
B [Mcal/m^2/hr]	1.899	6.094	2.157	1.177	0.112	7.601	6.349
C [Mcal/m^2/hr]	−0.373	−0.892	−0.388	−0.300	−0.015	−2.405	−1.272
D [Mcal/m^2/hr]	−25.661	−19.947	−22.065	−13.959	−25.300	−14.705	−27.323
E [Mcal/m^2/hr]	−10.424	−21.603	−28.118	−23.894	−19.629	−35.997	−11.099
z^* [m]	1.06	1.13	1.75	1.63	0.60	1.78	1.13
F_{H_2} [kg/hr]	3788	3944	3494	4211	3943	3954	3511
F_{stm} [ton/hr]	59.0	61.7	54.6	61.1	38.8	52.6	55.2
Q_{SMR} [Gcal/hr]	103.6	109.0	96.8	116.6	105.5	108.1	108.4
Q_{fuel} [Gcal/hr]	58.5	67.7	58.3	68.0	63.9	66.9	52.4
Q_{fuel}/Q_{ref} [%]	56.5	62.1	60.2	58.3	60.5	61.9	48.4

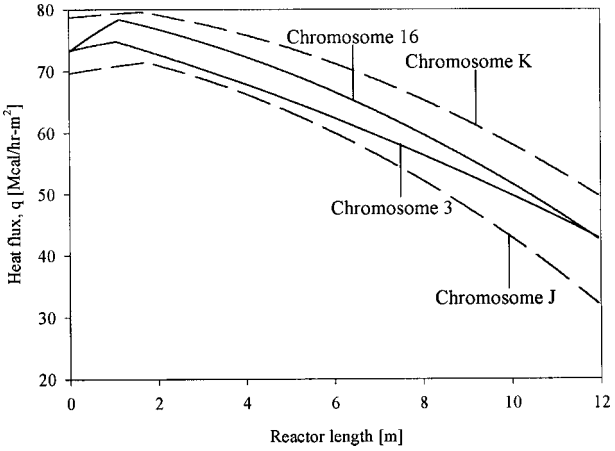

Fig. 9 Optimal heat flux profiles on reformer tubes for selected chromosomes of the Pareto-optimal set in Figs. 7 and 10

The variables, $(H/C)_{in}$ and $(S/C)_{in}$, as shown by the random scatter of their values with increasing F_{H_2} (Figs. 8(c) and (d)), appear to have negligible effects on H_2 production. These two variables, however, have major influence on steam generation (Fig. 8(e) and (f)). It is important to note that while $(H/C)_{in}$ and $(S/C)_{in}$ exhibit distinct trends with increasing F_{stm}, there remains a high degree of variation in F_{stm} for the same value of either of them. This may be explained by considering chromosomes 3 and 16 (see Table 2). Both chromosomes share the same values of $(H/C)_{in}$ and $(S/C)_{in}$, but hydrogen production and steam generation are higher in the case of chromosome 16 at the expense of an increased reformer duty. This can be attributed to the different heat flux profiles in the reformer, as described by the decision variables A to E and z^* according to Eq. (12), for the two chromosomes. These two heat flux profiles are illustrated in **Fig. 9**. For the same heat flux at the inlet, the profile for chromosome 16 rises more rapidly to attain a higher maximum heat flux. The heat flux profiles become identical again at the tube exit. In this manner, more heat duty is supplied to the process gas in the initial part of the reformer tube where the bulk of the reactions take place, to drive the forward reforming reactions (Eqs. (1) and (3)) so that higher H_2 production and steam generation can be achieved.

Operation of industrial hydrogen plants are subject to changes in methane flow rate, F_{CH_4}, allowable tube wall temperature, $T_{w,max}$ and catalyst activity. Effect of these on the multi-objective optimization is now studied. **Figure 10** shows the variation of the Pareto-optimal set for ±10% change in F_{CH_4}. For ease of comparison, 20 chromosomes have been selected from each solution set, and plotted against the values of the objectives in the ordinate axis. When F_{CH_4} is increased from 90% to the base case, more H_2 production and steam generation are possible, coupled with a proportionate increase in the reformer duty. This is consistent with our expectations since higher F_{CH_4} implies a greater extent of reaction taking place in the reformer, hence producing more H_2, and a greater amount of recoverable energy in the process gas at the reformer outlet, thus generating more steam. On the other hand, when F_{CH_4} is further increased to 110%, more H_2 production is achieved while steam generation remains

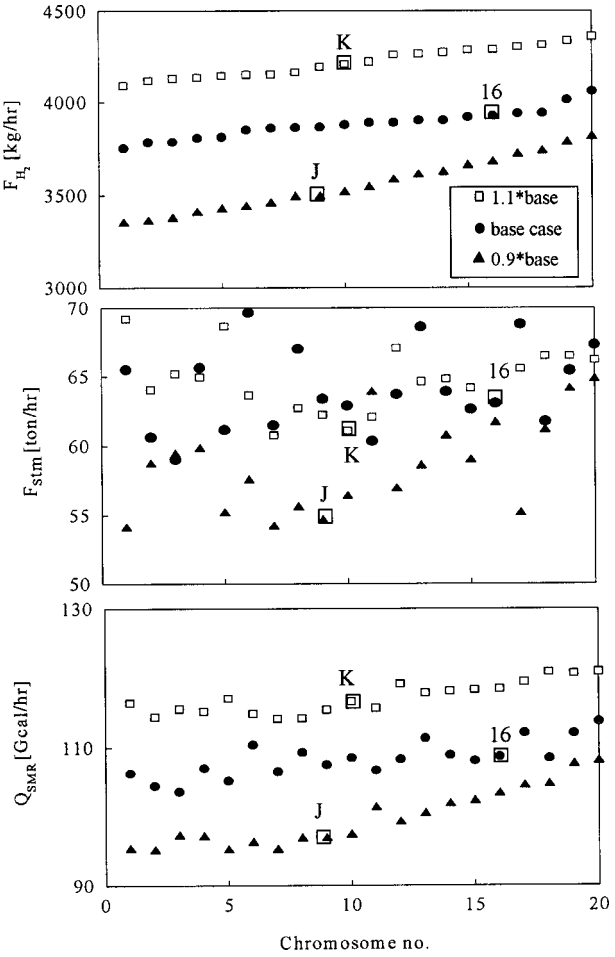

Fig. 10 Effect of methane feed rates, F_{CH_4}, on the optimal solutions for three objectives

comparable to that of the base case. This inability to achieve increased steam generation is attributed to the constraints on the heat duties of the two exchangers downstream of the reformer (Eq. (9)). The optimal solutions involve heat duties within 3% and 1% of $Q_{E1\,max}$ and $Q_{E2\,max}$, respectively. Furthermore, both increased H_2 production and greater steam generation were achieved when the constraints on the exchanger duties were removed. The reformer heat flux profiles of chromosomes J, K and 16 (Fig. 10) are shown in Fig. 9. The heat flux at any point of the reformer is higher with a greater F_{CH_4}, consistent with the need for more duty to drive forward the reforming reactions.

Changes in catalyst activity, for various reasons such as coking, poisoning, sintering or thermal aging, are to be expected in the normal course of plant operation. From an industrial perspective, the catalyst in the steam reformer, HT and LT shift converters is replaced after an average of, respectively, 3.5, 5 and 10 years on-line. A reduction in catalyst activity is accounted for by multiplying the rate constants of the reforming and shift reactions in the reformer and HT and LT shift converters by factors of 0.02, 0.0285 and 0.057, respectively, to reflect the relative rates of deactivation of catalyst in the three reactors. In addition, the constraint on the reformer heat duty supplied by external fuel (Eq. (19)) has been modified to

$$\frac{Q_{\text{fuel}}}{Q_{\text{SMR}}} \geq 0.43 \tag{21}$$

This modification is made in order to obtain optimized solutions with a range for reformer heat duty, Q_{SMR}, similar to that of fresh catalyst, to facilitate comparison between the solutions obtained for fresh and deactivated catalyst. With deactivated catalyst, a higher methane leakage from the reformer will increase the heating value of the PSA off-gas. It follows that a greater proportion of a fixed Q_{SMR} can be provided for by the off-gas with deactivated catalyst, as compared to fresh catalyst, therefore reducing the fraction supplied by external fuel. Thus if the said constraint (Eq. (19)) was kept unchanged for optimization with deactivated catalyst, the solutions would exhibit an increased Q_{SMR}, solely to meet the constraint. These solutions thus fail to reflect the true influence of catalyst deactivation on the optimized results. The sensitivity of the Pareto to the effect of catalyst deactivation is shown in **Fig. 11**. Both H_2 and steam production are observed to decrease with catalyst deactivation, while the reformer heat duty remains comparable with that of fresh catalyst. In addition, for the same Q_{SMR}, less external fuel needs to be supplied with deactivated catalyst, as a larger fraction of Q_{SMR} is supplied by the off-gas. Catalyst deactivation also affects the life of the reformer tubes. With deactivated catalyst, the heat supplied is used to increase the sensible heat of the process gas rather than to propagate the reforming reactions, resulting in higher wall temperatures. For example, chromosomes 16 (fresh catalyst) and N (deactivated catalyst) (Fig. 11) are comparable in terms of reformer heat duty, but the maximum reformer tube (outer) wall temperature, $T_{w,max}$, is 9.2°C higher in the latter case. As tube life is so highly sensitive to variations in the maximum tube wall temperature, $T_{w,max}$, that an increase in $T_{w,max}$ by 10°C shortens tube life by half (Rostrup-Nielsen, 1984), catalyst deactivation will have an adverse effect on tube life if operating variables are not adjusted to compensate.

As mentioned above, the life of a reformer tube is very sensitive to variations in $T_{w,max}$. The effect of the operational constraint on the maximum allowable tube (outer) wall temperature, $T_{w,max}$, on the Pareto is shown in **Fig. 12**. For better clarity, the optimal chromosomes have been projected onto representative two-dimensional planes. The upper limit on $T_{w,max}$ constrains the temperature the process gas can attain at the reformer outlet, dictating the extent of the reforming and shift reactions occurring in the reformer and thereby influ-

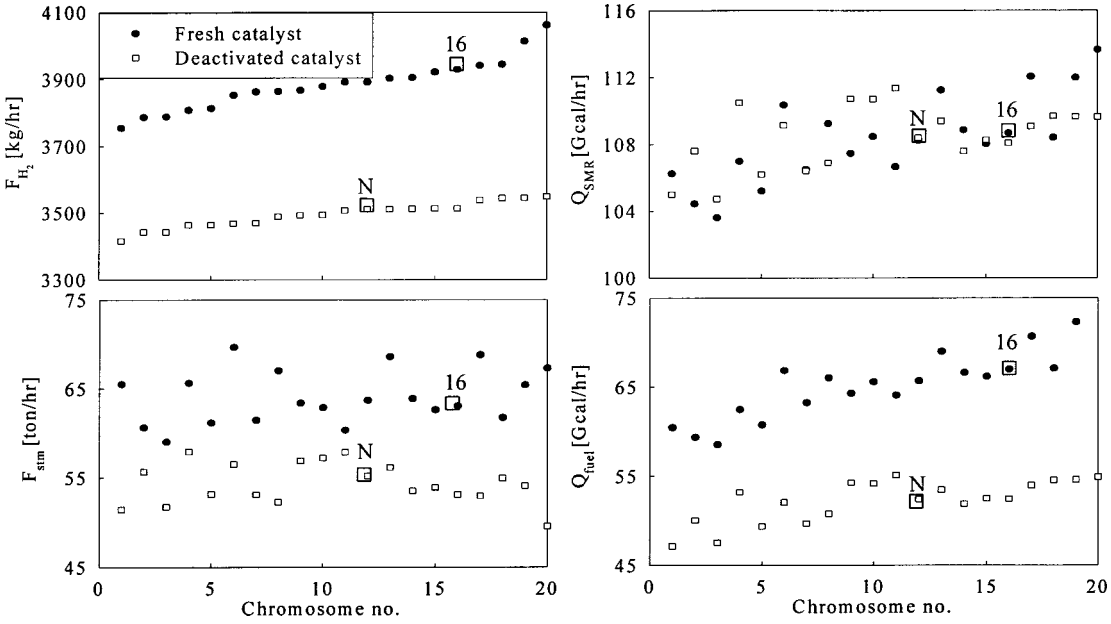

Fig. 11 Effect of catalyst deactivation on the optimal solutions for three objectives

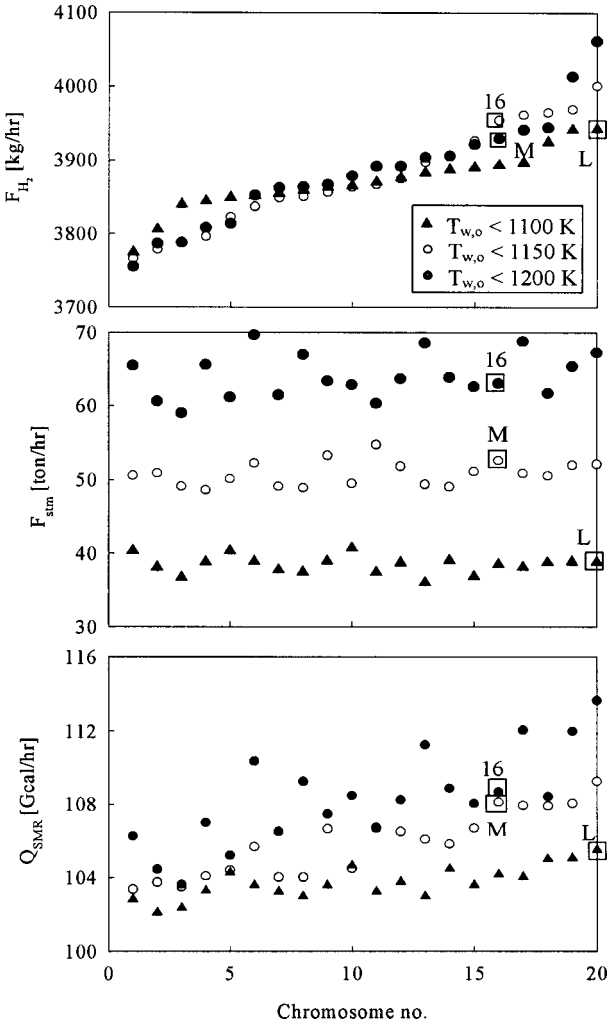

Fig. 12 Effect of constraint on reformer tube wall temperature on the optimal solutions for three objectives

encing the objective functions. Therefore, with a higher $T_{w,max}$ more heat duty may be supplied to the reformer to result in higher conversion of methane and increased production of H_2 and steam.

Conclusions

Operation of industrial hydrogen plants is optimized by considering multiple objective functions—maximization of hydrogen and steam production while minimizing reformer duty for a specified feed flow rate to the plant. The heat flux profile on reformer tubes is treated as an additional decision variable to provide greater scope for optimization. A nondominated sorting genetic algorithm (NSGA) is successfully used for both two and three objective functions. The results from two-objective optimization show that significant improvement in the objectives can be achieved by choosing, optimally, a heat flux profile on reformer tubes instead of just furnace gas temperature. Hydrogen plant operation can also be optimized for three objectives to yield additional meaningful information, with no increase in computational time. Optimization is performed for different feed flow rate, tube wall temperature and catalyst activity. The results can be used for adjusting salient operating parameters with a change in any of these conditions.

Appendix: The NSGA Technique

The Nondominated Sorting Genetic Algorithm (NSGA), developed by Srinivas and Deb (1995) to solve multi-objective optimization problems, generates a set of solutions which are nondominating over each other. Two solutions are said to be nondominating if an improvement in one of the objectives is accompanied by a deterioration in one (or more) of the other objec-

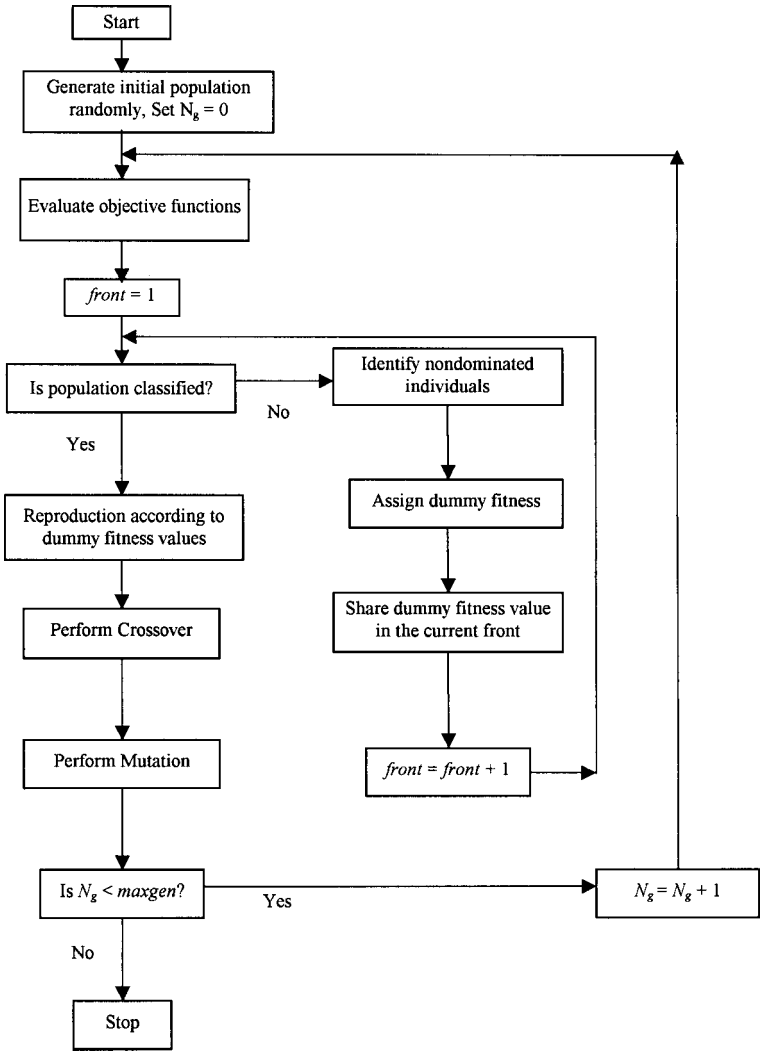

Fig. A1 A flow chart of NSGA (adapted from Mitra *et al*., 1998)

tive function(s) when moving from one point to another. The final set of nondominating solutions is referred to as a Pareto-optimal set. The NSGA differs from the original GA (Goldberg, 1989; Deb, 1995) in the way the selection operator works. In the former, the randomly generated solutions are sorted into imaginary enclosures called fronts. All the chromosomes within the same front are mutually nondominating. Each front is assigned a progressively lower common (dummy) value of the fitness function. Then, each chromosome in any front is assigned an individual value of the fitness function, which is obtained by dividing the dummy fitness value for the front by the niche count of the individual chromosome. (The niche count is a parameter proportional to the number of chromosomes in the neighbourhood of this chromosome within the same front.) This action helps to spread out the chromosomes and to maintain the diversity of the gene pool. All other operations performed are similar to those in the traditional GA. A flow chart of the NSGA is shown in **Fig. A1**.

Nomenclature

A–E	=	constants defined in Eq. (12)	
F	=	total molar feed rate	[kmol/hr]
F_{H_2}	=	flow rate of hydrogen from the unit	[kg/hr]
F_{max}	=	maximum total molar feed rate	[kmol/hr]
F_{stm}	=	flow rate of export steam	[ton/hr]
$(H/C)_{in}$	=	recycle hydrogen/methane molar ratio in the feed	
L	=	total length of the steam reformer tubes	[m]
$P_{SMR,in}$	=	pressure at the inlet to the steam reformer	[kPa]
q	=	heat flux at any location on the reformer tubes	[Mcal $hr^{-1}m^2$]
Q	=	heat duty	[Gcal/hr]
$Q_{ei\ max}$	=	maximum heat duty of heat exchanger E1 (i = 1) or E2 (i = 2)	
Q_{SMR}	=	heat duty required by the steam reformer	[Gcal/hr]
Q_{fuel}	=	heat duty supplied by external fuel	[Gcal/hr]
$(S/C)_{in}$	=	steam/methane molar ratio in the feed	
T_{dew}	=	dew point temperature of the bulk gas	[K]
$T_{w,max}$	=	temperature of the outer tube wall	[K]
$T_{SMR,in}$	=	temperature at the inlet to the steam reformer	[K]
$T_{HTS,in}$	=	temperature at the inlet to the HT shift converter	[K]
$T_{LTS,in}$	=	temperature at the inlet to the LT shift converter	[K]
y_i	=	mole fraction of the component i in the bulk gas	
z	=	axial location in the reformer tube	[m]
z^*	=	axial location in the reformer tube where the maximum point heat flux occurs	[m]

α	=	upper limit on the fraction of reformer heat duty supplied by external fuel
β	=	multiplication factor for the forward rate constants in the steam reformer and shift converters to account for catalyst deactivation
ΔH_r	=	heat of reaction [kcal/kmol]
ν	=	dimensionless distance within the half thickness of the catalyst pellet ($\nu = 0$ at catalyst surface)

<Subscript>

E1	=	steam generator
E2	=	preheater for boiler feed water
HTS	=	high-temperature shift converter
LTS	=	low-temperature shift converter
SMR	=	steam methane reformer

Literature Cited

Bhaskar, V., S. K. Gupta and A. K. Ray; "Applications of Multiobjective Optimization in Chemical Engineering," *Rev. Chem. Eng*., **16**, 1–54 (2000a)

Bhaskar, V., S. K. Gupta and A. K. Ray; "Multiobjective Optimization of an Industrial Wiped-Film PET Reactor," *AIChE J.*, **46**, 1046–1058 (2000b)

Chlendi, M., D. Tondeur and F. Rolland; "Method to Obtain a Compact Representation of Process Performances from a Numerical Simulator: Example of Pressure Swing Adsorption for Pure Hydrogen Production," *Gas Sep. Purif*., **9**, 125–135 (1995)

Deb, K.; Optimization for Engineering Design: Algorithms and Examples, Prentice-Hall of India, New Delhi, India (1995)

Elnashaie, S. S. E. H. and F. M. Alhabdan; "Mathematical Modelling and Computer Simulation of Industrial Water-Gas Shift Converters," *Math. Comput. Model*., **12**, 1017–1034 (1989)

Elnashaie, S. S. E. H. and S. S. Elshishini; Modelling, Simulation and Optimization of Industrial Catalytic Fixed-Bed Reactors, pp. 342–364, Gordon and Breach, Amsterdam, the Netherlands (1993)

Garg, S. and S. K. Gupta, "Multiobjective Optimization of a Free Radical Bulk Polymerization Reactor Using Genetic Algorithm," *Macromol. Theor. Simul*., **8**, 46–53 (1999)

Goldberg, D. E.; Genetic Algorithms in Search, Optimization, and Machine Learning, Addison-Wesley, Reading, USA (1989)

King, D. L. and C. E. Bochow, Jr.; "What Should an Owner/Operator Know When Choosing an SMR/PSA Plant?," *Hydrocarb. Process*., **79**, 39–48 (2000)

Mitra, K., K. Deb and S. K. Gupta; "Multiobjective Dynamic Optimization of an Industrial Nylon 6 Semibatch Reactor Using Genetic Algorithm," *J. Appl. Polym. Sci*., **69**, 69–87 (1998)

Rajesh, J. K., S. K. Gupta, G. P. Rangaiah and A. K. Ray; "Multiobjective Optimization of Steam Reformer Performance Using Genetic Algorithm," *Ind. Eng. Chem. Res*., **39**, 706–719 (2000)

Rajesh, J. K., S. K. Gupta, G. P. Rangaiah and A. K. Ray; "Multiobjective Optimization of Industrial Hydrogen Plants," *Chem. Eng. Sci*., **56**, 999–1010 (2001)

Rostrup-Nielsen, J. R.; "Catalytic Steam Reforming," Catalysis—Science and Technology Vol. 5, A. R. Anderson and M. Boudart, eds., pp. 1–117, Springer, Berlin, Germany (1984)

Singh, C. P. P. and D. N. Saraf; "Simulation of Side Fired Steam-Hydrocarbon Reformers," *Ind. Eng. Chem. Proc. D. D*., **16**, 313–319 (1979)

Srinivas, N. and K. Deb; "Multiobjective Function Optimization Using Nondominated Sorting Genetic Algorithms," *Evol. Comput*., **2**, 221–248 (1995)

Xu, J. and G. F. Froment; "Methane Steam Reforming, Methanation and Water-Gas Shift: I. Intrinsic Kinetics," *AIChE J*., **35**, 88–96 (1989a)

Xu, J. and G. F. Froment; "Methane Steam Reforming: II. Diffusional Limitations and Reactor Simulation," *AIChE J*., **35**, 97–103 (1989b)